Progress in NUCLEAR SCIENCE and TECHNOLOGY, Vol. 1, p.114-117 (2011)

ARTICLE

Study of neutron and photon production cross sections for second cancer risk assessment in heavy-ion therapy

Yusuke UOZUMI[1*], Hiroki IWAMOTO[1], Yusuke KOBA[1], Naruhiro MATSUFUJI[2], Toshiya SANAMI[3], Daiki SATOH[4], Nobuhiro SHIGYO[1], Masashi TAKADA[2], Masahiko UEYAMA[1], Masakatsu YOSHIOKA[1] Mamoru BABA[5]

[1]*Kyushu University, 744, Motooka, Nishi-ku, Fukuoka 819-0395, Japan*
[2]*National Institute of Radiological Sciences, Anagawa, Inage, Chiba 263-8555, Japan*
[3]*High Energy Accelerator Research Organization KEK, Oho, Tsukuba, Ibaraki 305-0801, Japan*
[4]*Japan Atomic Energy Agency, Tokai, Naka, Ibaraki 319-1195, Japan*
[5]*Tohoku University, Aramaki, Aoba-ku 980-8578, Miyagi, Japan*

In the heavy-ion radiotherapy, considerable discussion has been attracted regarding the potential for second cancer induction by secondary neutrons produced in primary heavy-ion fragmentation. It is needed to develop a Monte-Carlo simulation tool to estimate neutron doses and the photon contribution. Since it is notoriously hard to reproduce the spectral cross sections of neutrons and photons by simulations, we have planned experiments to measure energy-angle double-differential cross sections of nuclear reactions. Several simulation studies have been conducted to realize experiments at the synchrotron HIMAC of NIRS, Japan. Expected spectral cross sections of neutrons and photons are discussed by using Monte-Carlo simulation codes, PHITS and EGS5.

KEYWORDS: heavy-ion radiotherapy, second cancer induction, neutron, photon, cross section, PHITS, EGS5, Monte-Carlo simulation

I. Introduction

A heavy-ion beam offers an excellent advantage in radiotherapy because of the conformation of a high radiation dose to a target volume thanks to the presence of the Bragg peak. The heavy-ion therapy, therefore, can selectively damage tumor tissues while sparing the surrounding healthy tissues, and allows the lower whole-body dose compared with the conventional radiotherapy which uses photon or electron beams. For instance, the intensity-modulated photon radiotherapy can produce a high dose region, but have a high integral dose deposition in the health tissues. This integral dose may cause late side effects and the possible secondary cancer.

Neutrons produced by the primary beam in proton and heavy-ion therapies could contribute to the integral dose. Undesired exposure from secondary neutrons has attracted considerable discussion in recent years. [1)] Since neutrons have a large quality factor, even a small physical dose can results in serious biological effects. Low neutron doses are known to have a high potential for carcinogenesis. The dose equivalent deposited by these neutrons is usually not considered in the treatment planning. It is important to develop a method to assess the potential of second cancer induction by secondary neutrons.

In many clinical proton therapy facilities, secondary neutron doses were measured with dosimeters. However, these results vary greatly. The cause of disagreements has been attributed to difficulties in neutron dose measurements in mixed radiation fields. Variations would be introduced from different measurement technique and different beam geometries. A Monte-Carlo simulation approach has been shed light as an alternate for the dose estimation and a guide for more reliable measurement.

There are some simulation tools available which can offer opportunity to estimate nuclear reaction cross sections. In order to verify their predictive ability, there are strong requests on neutron spectral cross sections. Although there are several measured data, [2–5)] most of them are for heavy-nuclear targets aiming at radiation shielding study. Only a few data exist for tissue constituent element targets. Moreover it is widely known that theoretical calculations give poor accounts to cross sections on light target nuclei. Theoretical predictions are inconsistent between different calculation codes.

Along the above context, we have planned experiments to measure energy-angle double-differential cross sections. Measurements of photon production cross sections are also planned to make a comparison with actual dose measurements. To realize the experiment, serious simulation studies are needed in advance to the experiment. The present article describes some typical results of simulation studies using codes PHITS [6)] and EGS5 [7)].

II. Outline of planned experiment

The experiments are planned to be made at NIRS, Japan. Heavy-ions such as carbon, nitrogen, and oxygen will be accelerated up to 200 MeV/u or higher by the synchrotron HIMAC [8)]. The beam is transported, and bombards a carbon plate target located in the PH2 course of the experimental hall. The experimental setup is shown in **Fig. 1.** The beam emerges from the vacuum duct through a 100-μm-thick aluminum window, and impinges on the target placed in

*Corresponding Author, E-mail:uozumi@nucl.kyushu-u.ac.jp

atmosphere. After passing through the target, the beam traverses a trigger detector, which is an NE102A plastic scintillator plate of 0.5 mm thick, 150 mm wide and 200 mm height. The trigger detector will provide the start signal for the TOF measurement, and the number of incident particles. After pass through the target, the beam flies in air and stops at a beam dump placed about 10 m downstream from the target.

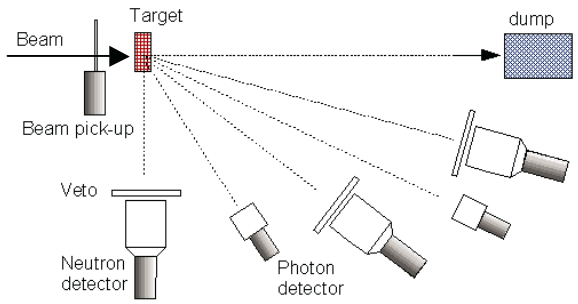

Fig.1 Typical setup of apparatus.

Energies of emitted neutrons are measured with NE213 liquid organic scintillators, of which the dimension of 12.7 cm thick and 12.7 cm in diameter by the TOF technique. The response functions of the present NE213 liquid organic scintillator had been already established through several experiments and simulations. Measurements for photons are carried out by using both NE213 and BGO crystal, having a 2-inch edge-length, counters. Energies of photons are analyzed by the conventional pulse height technique.

Scintillators of NE213 are placed at several angles from 5° to 150° to measure angular distributions. The target is a carbon sample 8 mm thick and 50 mm in diameter. The distance between the sample and each detector should be about 0.5 m for low-energy, and about 5 m for high-energy measurements. A 10 mm thick NE102A plastic scintillator as a veto detector is set in front of each detector to eliminate charged particles. Gamma-ray events can be discriminated using the two gate integration method [9] since NE213 liquid organic scintillators are sensitive to not only neutrons but also gamma-rays. Comparison between charge spectrum with the prompt-gate and that with the delayed-gate enables to discriminate neutron events and gamma-rays ones.

Resultant spectra of charge-integration of each NE213 detector must be calibrated in terms of the electron-equivalent light-output. For the calibrations of the low-energy (a few MeV) part of spectra, the gamma-rays Compton edges of ^{60}Co and Pu-Be sealed sources are converted into light-unit with the semi-empirical formula by Dietze et al.[10] For the calibrations of the higher energy domain, neutron energies identified by the TOF between the spallation target and neutron detectors were converted into light-unit by the empirical equation by Cecil et al.[11]

$$T_e = 0.83T_p - 2.82\left[1.0 - \exp(0.25T_p 0.93)\right], \qquad (1)$$

where T_p, T_e are proton and electron energy in an NE213 scintillator, respectively. The peak channel of the charge spectra was used as corresponding charge-integration values.

III. Simulation

1. Spectra of secondary radiations

The simulation code PHITS was used to estimate spectral energy distributions of neutrons, photons, charged particles, and pions from heavy-ion interactions at a relativistic energies. In the simulation, the carbon ions of 290 MeV/u hit target nuclei in the laboratory frame, and emitted radiation flux were calculated at angles of detector positions. As target nuclei, we choose carbon, oxygen, and water.

2. Charged particles emission from secondary neutrons

Secondary neutrons will cause a certain amount of dose in the patient body and the external field. The knowledge on this distribution is useful for effective planning of the experiment. We carried out calculations of charged particle fluxes from neutron-water interaction at energies ranging from 2 to 200 MeV by the use of the code PHITS. Firstly, charged particle productions were simulated with neutrons impinging a water slab. The energy deposit by charged particles at the surface of the column was calculated. Secondly, the dose distributions can be estimated from energy spectra and the conversion coefficients.

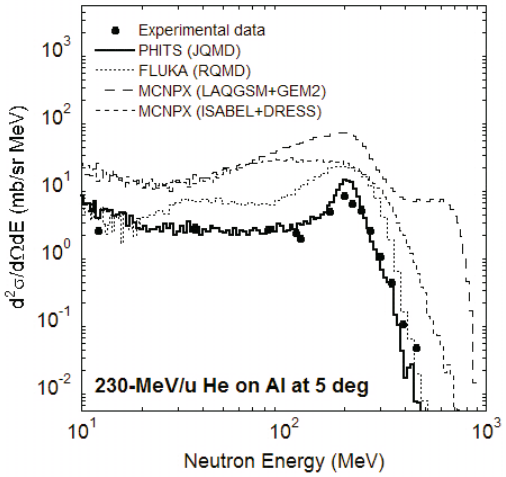

Fig. 2 Comparison of neutron energy spectra between different models and experiments.

3. Neutron detector response functions

In this experiment, the SCINFUL-QMD [12] calculations adjusted to reproduce experimental data with light attenuation are used as response matrix elements below 30 MeV of the incident energy for all neutron detectors since there are no experimental data below 30 MeV.

4. Photon detector response functions

We used the code EGS5 to obtain the response functions of crystal scintillator detectors to gamma-rays of energies

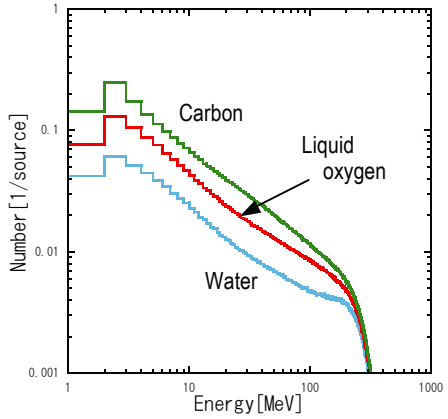

Fig. 3 Energy spectra of neutrons from carbon, liquid oxygen and water with 290-MeV/u C beam.

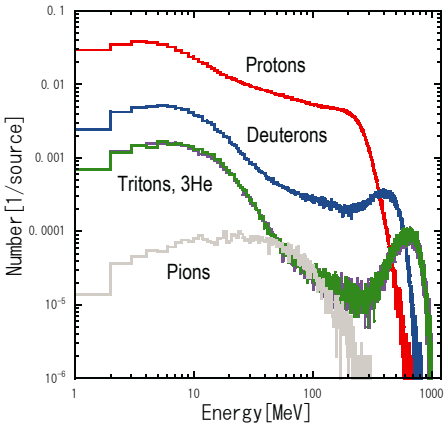

Fig. 4 Energy spectra of charged particles from C + water interaction at 290 MeV/u.

from 0.2 to 20 MeV. The detector is surrounded by a solid lead shielding of 5 to 10 cm thick. The response is needed for the unfolding analyses. Therefore, the efficiency of the shielding, and the contribution of photon scattered off the shielding was also analyzed.

IV. Results and discussion

As depicted above, simulation calculations were performed intensively on various issues. Although all of the results are essential to realize the planned experiment, some of typical results are presented in this section.

1. Spectra of secondary radiations

For instance, spectral neutron distributions are compared between PHITS and other simulation codes, FLUKA[13] and MCNPX [14] for the He+Al reaction at 230 MeV/u in **Fig. 2**. Overall large discrepancies appear. These greatly distributed results should suggest the importance of real measurements, which offer opportunity to improve the predictive ability of theoretical calculations.

In **Fig. 3** are displayed PHITS results of neutron fluxes expected from a source of each reaction, i.e., the carbon, liquid oxygen and water bombarded by a 290-MeV/u carbon ion. All of spectral shapes are very similar. The largest flux of a few MeV or less should be noticed, because the radiation waiting factor is the highest in this energy range. Since this energy is the lowest limit for the standard TOF technique, no data has been obtained so far. Intensive efforts should be paid to take data in this energy domain.

In **Fig. 4**, flux distributions are displayed for protons, deuterons, tritons, ^{3}He and pions from the 290-MeV/u carbon induced reaction. The proton yield is almost 90% of all charged particles, and very similar amount to that of neutrons. The deuteron yield is the second most, but less than 10% of the proton yield. Other particle yields would be negligibly small.

The neutron and photon fluxes are compared for a thin water slab of 20-mm depth and 100-mm depth bombarded by 290-MeV/u carbon ions, in **Figs. 5** and **6**, respectively. Significant increases appear in the lowest energy domain for both neutrons and photons with increasing water slab thickness. The low energy flux is sensitive to the exposure conditions, which implies that low energy data is highly important for more accurate dose estimations.

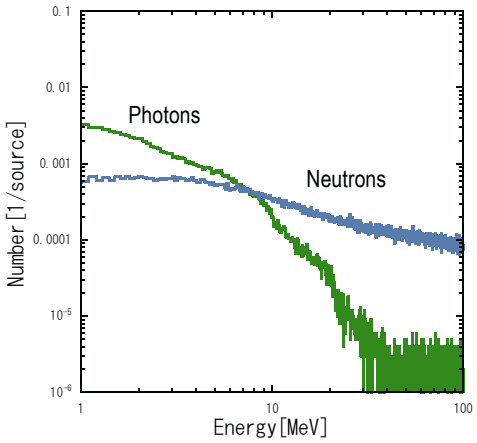

Fig. 5 Energy spectra of neutrons and photons from 20-mm thick water with 290-MeV/u C beam.

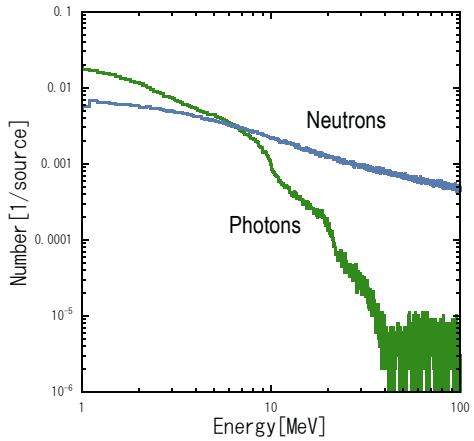

Fig. 6 Energy spectra of neutrons and photons from 100-mm thick water with 290-MeV/u C beam.

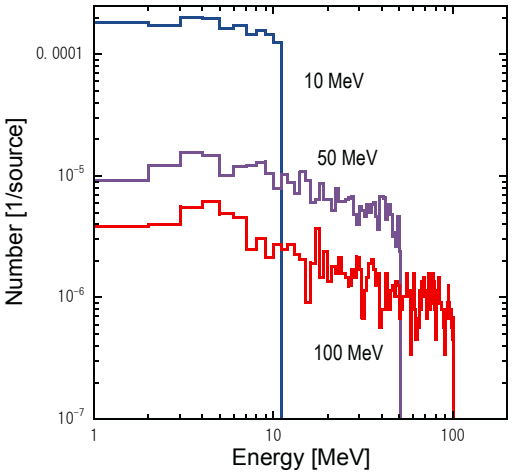

Fig. 7 Energy spectra of protons from neutron + water interaction at 10, 50 and 100 MeV.

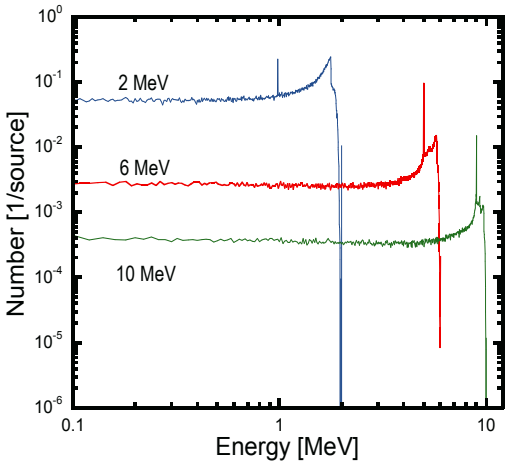

Fig. 8 Energy depositions in 10-cm-thick water from photon + water interaction at 2, 6 and 10 MeV.

The target thickness dependence was investigated with water targets of 2, 4, and 10 cm thick. In **Fig. 7** are shown proton fluxes from a 10-cm water slab bombarded by neutrons of energies 10, 50 and 100 MeV. Energy depositions from photons to water are displayed in **Fig. 8** for photons of energies 2, 6 and 10 MeV. In the both cases, the proton yield from the lower energy radiation incidences increase with increasing target thickness more than that from the higher energy radiations. This implies that low-energy radiations affect sensitively to geometrical conditions, which causes variations of measured neutron doses.

V. Conclusion

For accurate assessment of a secondary cancer risk in carbon-ion therapy, detailed simulation tasks were performed to realize real experiments for double-differential cross sections of neutron and photon productions from carbon- induced reactions on tissue element nuclei. The expected spectral cross sections were investigated with the simulation tool of PHITS. The code EGS5 was also used to study the photon interactions. Contributions of possible secondary radiations to the spatial dose distribution were also calculated. These results revealed that the neutrons and photons of low energies cause large doses and serious geometric sensitivity. The importance of measurements has been recognized in the energy domain down to a few MeV, where the TOF technique is difficult due to the poor n/γ discrimination. The experiment is ready in October 2009.

Acknowledgment

Authors gratefully acknowledge Dr. T. Murakami, Dr. T. Nakamura and Dr. Y. Iwata for useful information and discussion. The study is assigned as HIMAC-P252.

References

1) Brenner, D. J. and Hall, E. J., Secondary neutrons in clinical proton radiotherapy: A charged issue, Radiotherapy and Oncology 86 (2008) 165-170; Xu, X. G., Bednarz, B., Paganetti, H., A review of dosimetry studies of external-beam radiation treatment with respect to second cancer induction, Phys. Med. Biol. 53 (2008) 193-242; and references therein.
2) Madey, R., Inclusive neutron spectra at 0° from Nb-Nb collisions at 800 MeV/nucleon, Phys. Rev. C38 (1988) 184.
3) Cecil, R. A., Inclusive neutron production by 337 MeV/nucleon neon ions on carbon, aluminum, copper, and uranium, Phys. Rev. C24 (1981) 2013.
4) Madey, R., Inclusive neutron cross sections at forward angles from Nb-Nb and Au-Au collisions at 800 MeV/nucleon, Phys. Rev. C42(1990) 1068.
5) Baldwin, A. R., Madey, R., et al., Phys. Rev. C46 (1992) 258.
6) Iwase, H., Niita, K., Nakamura, T., Development of General-Purpose Particle and Heavy Ion Transport Monte Carlo Code, J. Nucl. Sci. Technol., 39 (11) (2002) 1142– 1151.
7) Namito, Y. and Hirayama, H., Proceedings of the International Workshop on EGS, KEK Proceedings 2005-3 (2005).
8) Sato, K., et al., Performance of HIMAC, Nucl. Phys. A588 (1995) c229-c234.
9) Moszynski, M., et al., Identification of different reaction channels of high energy neutrons in liquid scintillators by the pulse shape discrimination method, Nucl. Instrum. and Meth. in Physics Research Section A 343 (2-3) (1994) 563–572.
10) Dietze, G., Klein, H., Nucl. Instrum. Methods. 193 (1982) 549.
11) Cecil, R. A., Anderson, B. D., Madey, R., Nucl. Instr. Meth. 161 (1979) 439.
12) Satoh, D., et al., SCINFUL-QMD: Monte Carlo Based Computer Code to Calculate Response Function and Detection Efficiency of a Liquid Organic Scintillator for Neutron Energies up to 3 GeV, JAEA-Data/Code 2006-023, Japan Atomic Energy Agency (JAEA) (2006).
13) Ferrari, A., Sala, P.R. Fasso, A. and Ranft, J., CERN 2005-10 (2005).
14) Pelowitz, D. B., editor, MCNPX User's Manual Version 2.6.0, LA-CP-07-1473, Los Alamos National Laboratory (2008).